UC San Diego

UC San Diego Previously Published Works

Title

Complete inhibition of a polyol nucleation by a micromolar biopolymer additive

Permalink

https://escholarship.org/uc/item/0sf2p4qp

Journal

Cell Reports Physical Science, 3(2)

ISSN

2666-3864

Authors

Wen, Xin

Wang, Sen

Ramji, Robert

et al.

Publication Date

2022-02-01

DOI

10.1016/j.xcrp.2021.100723

Copyright Information

This work is made available under the terms of a Creative Commons Attribution License, available at https://creativecommons.org/licenses/by/4.0/

Peer reviewed

eScholarship.org Powered by the California Digital Library
University of California

Author Manuscript

Author Manuscript

Author Manuscript

Author Manuscript

HHS Public Access

Author manuscript

Cell Rep Phys Sci. Author manuscript; available in PMC 2022 March 08.

Published in final edited form as:

Cell Rep Phys Sci. 2022 February 16; 3(2): . doi:10.1016/j.xcrp.2021.100723.

Complete inhibition of a polyol nucleation by a micromolar biopolymer additive

Xin Wen[1,6,*], **Sen Wang**[1,7], **Robert Ramji**[2], **Luke O. Butler**[2], **Yelena Bagdagulyan**[1], **Audrey Kishishita**[1], **James A. Golen**[3], **Arnold L. Rheingold**[3,4], **Soo-Kyung Kim**[5], **William A. Goddard III**[5,*], **Tod A. Pascal**[2,3,*]

[1]Department of Chemistry and Biochemistry, California State University, Los Angeles, Los Angeles, CA 90032, USA

[2]ATLAS Materials Physics Laboratory, Department of NanoEngineering and Chemical Engineering, University of California, San Diego, La Jolla, CA 92093, USA

[3]University of California San Diego Materials Research Science and Engineering Center, University of California, San Diego, La Jolla, CA 92093, USA

[4]Department of Chemistry and Biochemistry, University of California, San Diego, La Jolla, CA 92093, USA

[5]Materials and Process Simulation Center, California Institute of Technology, Pasadena, CA 91125, USA

[6]Lead contact

[7]Present address: Department of Chemistry, California State University, Dominguez Hills, Carson, CA 90747, USA

SUMMARY

Preventing spontaneous crystallization of supersaturated solutions by additives is of critical interest to successful process design and implementation, with numerous applications in chemical, pharmaceutical, medical, pigment, and food industries, but challenges remain in laboratory and industry settings and fundamental understanding is lacking. When copresented with antifreeze proteins (AFPs), otherwise spontaneously crystallizing osmolytes are maintained at high supersaturations for months in over-wintering organisms. Thus, we here explore the inhibition phenomenon by AFPs, using persistent crystallization of a common sugar alcohol, D-mannitol, as

This is an open access article under the CC BY license (http://creativecommons.org/licenses/by/4.0/).

*Correspondence: xwen3@calstatela.edu (X.W.), wag@caltech.edu (W.A.G.), tpascal@ucsd.edu (T.A.P.).

AUTHOR CONTRIBUTIONS

X.W. and S.W. conceived the idea. X.W. directed the protein studies. Y.B. and A.K. performed the protein studies. S.W. and X.W. directed and performed crystallization and solids characterization studies. A.L.R. directed X-ray crystallography studies. J.A.G. and A.L.R. performed X-ray crystallography studies. T.A.P. directed the computational and theoretical studies, S.K.K. performed the ligand docking studies, R.R. performed the quantum calculations, and L.B. performed the MD simulations. X.W., T.A.P., and W.A.G. drafted the manuscript. All authors discussed the results and commented on the manuscript.

SUPPLEMENTAL INFORMATION

Supplemental information can be found online at https://doi.org/10.1016/j.xcrp.2021.100723.

DECLARATION OF INTERESTS

The authors declare no competing interests.

Author Manuscript Author Manuscript Author Manuscript Author Manuscript

a case study. We report experimentally that DAFP1, an insect AFP, completely inhibits D-mannitol nucleation. Computer simulations reveal a new mechanism for crystallization inhibition where the population of the crystal-forming conformers are selectively bound and randomized in solution by hydrogen bonding to the protein surface. These results highlight the advantages of using natural polymers to address crystallization inhibition challenges and suggest new strategies in controlling the nucleation processes.

Graphical Abstract

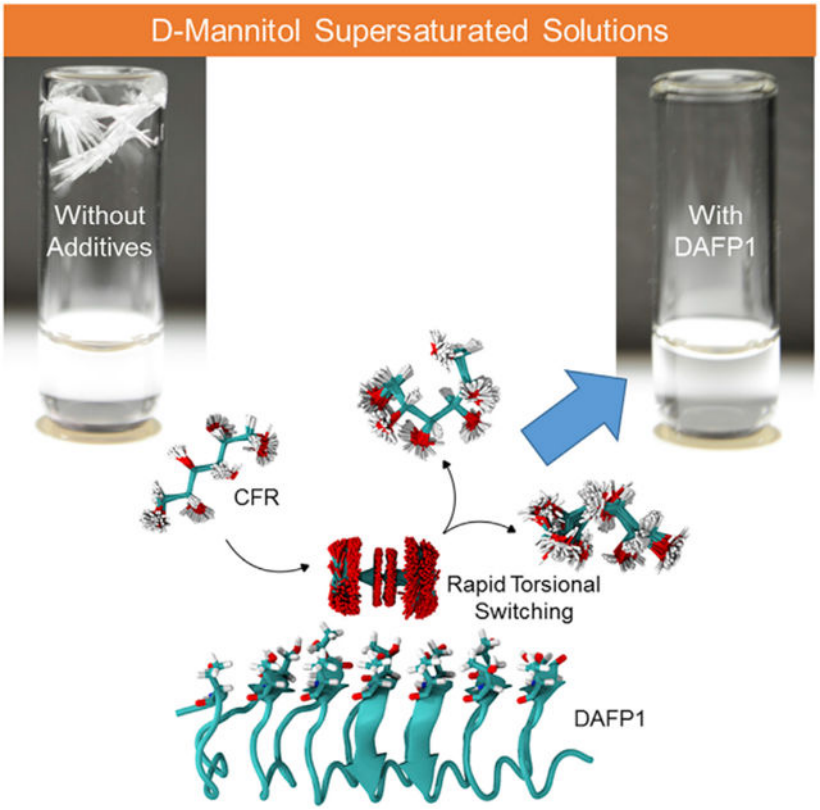

Preventing spontaneous crystallization of supersaturated solutions is important in industrial applications but remains a challenge with limited understanding. Wen et al. show that an insect antifreeze protein completely inhibits D-mannitol nucleation. Computer simulations reveal a dramatic reduction in the crystal forming rotamer population in solution mediated by the protein.

INTRODUCTION

Crystallization from solution is a ubiquitous phenomenon in nature and in industrial processes, making prevention of spontaneous crystallization of supersaturated solutions of critical interest for successful process design and implementation in various applications including chemical, pharmaceutical, medical, pigment, and food industries. Certain additives, such as tailor-made molecules and complexation agents,[1-3] have been reported to inhibit or slow down crystallization from supersaturated solutions. However, selection of such additives is a trial-and-error process, with the control often far from optimum

Author Manuscript Author Manuscript Author Manuscript Author Manuscript

and the concentrations required for the additives generally high (far above the micromolar level). Can spontaneous crystallization be completely suppressed from highly supersaturated solutions by a minute amount of additives over months at the nucleation stage? If such an additive exists, how can we find it and how would it function?

Nature has evolved ways to tackle this problem strategically. Antifreeze proteins (AFPs) evolved in many cold-adapted organisms (e.g., fishes, insects, plants, bacteria, and fungi) are known to have an extraordinary ability to suppress ice growth through binding to specific ice crystal surfaces.[4-7] Beetle AFPs usually have well-defined structures and are much more active than their counterparts in fish. For example, a hyperactive beetle AFP from *Dendroides canadensis* (DAFP1) is a 9 kDa β-helical protein with multiple 12- or 13-mer repeats including T-X-T (where X is any amino acid) and eight disulfide bonds with both its overall structure and ice-binding sites (IBSs) well-defined (Figure 1A).[6] In contrast, fish antifreeze glycoproteins (AFGPs) are intrinsically disordered and contain multiple repeats of the tripeptide A-A-T with the disaccharide β-D-galactosyl-(1→3)-N-acetyl-α-D-galactosamine (GalNAc) that are joined to the threonine residue through a glycosidic linkage (Figure 1 B).[8,9] Even more remarkably, AFPs have been shown to effectively control precipitation out of solution of certain non-ice like, low-molecular weight organic compounds, such as nucleosides,[10] monosaccharides,[11] and disaccharides.[6] These results imply additional functions for AFPs in cold-adapted organisms especially since AFPs coexist with high concentrations of osmolytes accumulated in cold-adapted organisms for survival of these organisms over the winter, where spontaneously crystallizing osmolytes can be maintained at high supersaturations without crystallization for months.[4-7] Serving as an important class of osmolytes, sugar alcohols (or polyols) can enhance the antifreeze activity of AFPs.[12] However, the role of AFPs on sugar alcohols is unknown.

Here, we choose D-mannitol [(2R,3R,4R,5R)-hexane-1,2,3,4,5,6-hexol] (Figure 1C) as a model polyol for several reasons. First, D-mannitol acts as a common cryoprotectant in cold-adapted organisms and is a common polyol in winter-hardy insects.[13] Furthermore, D-mannitol is the only common sugar alcohol that crystallizes spontaneously from solution.[7] Moreover, D-mannitol has many uses in a wide range of industries where control of its crystallization is critical. For example, because of its low glycemic index (GI) and safety for teeth, D-mannitol is utilized as reduced-sugar or sugar-free reformulations in the food industry.[14] D-mannitol is also a commonly used osmotic diuretic treatment to manage fluid build-up conditions (e.g., cerebral edema, increased intracranial pressure) in the medical industry.[15] In addition, D-mannitol is a popular excipient in solid formulations to stabilize active pharmaceutical ingredients in the pharmaceutical industry.[16]

Many uses of D-mannitol require the compound to remain in its aqueous solution without crystallization. In particular, as a parenteral obligatory osmotic diuretic, the crystallization of D-mannitol injection solution (approximately 15%–25% w/v) must be prevented.[17] However, D-mannitol solutions readily crystallize during regular storage and manufacturing (Figure 1D), in particular, when exposed to low temperatures. The crystallization of D-mannitol at lower temperatures limits its application as a key formulation excipient (approximately 10%–15% w/v) for frozen or freeze-dried protein drugs and mRNA

Author Manuscript Author Manuscript Author Manuscript Author Manuscript

vaccines.[18,19] The identification of an effective inhibitor for D-mannitol nucleation is thus imperative for its many industrial uses, but little progress has been achieved so far.

In this work, we show that DAFP1 is an extremely efficient inhibitor of D-mannitol nucleation at highly supersaturated conditions, with complete inhibition observed experimentally over 3 years using only micromolar levels of DAFP1 additive. Based on extensive computer simulations and free energy analysis, we discovered a new mechanism that explains this inhibition, predicting that DAFP1 reduces the population of the crystal forming rotamer by three orders of magnitude, which we predict would extend the crystal induction time to 75 years.

RESULTS AND DISCUSSION

Crystallization of D-mannitol

There are several different crystalline forms of D-mannitol, but slow evaporation of D-mannitol aqueous solution yields pure β-form D-mannitol, the most stable form.[20] Unfortunately, this also often results in mixtures of small crystals that are not suitable for accurate induction time determination. To solve this problem, we tested many crystallization conditions of D-mannitol and found that storing the supersaturated solutions of D-mannitol at 4°C (indeed a common storage mistake for commercially available D-mannitol solutions) yields high-quality pure β-form D-mannitol crystals reproducibly with respect to the induction time and the sizes and shapes of the resulting crystals. This condition was used throughout this study.

Next, we studied the inhibition of D-mannitol crystallization using DAFP1 (Figure 1A), a beetle AFP from *Dendroides canadensis*.[6] Fish AFGP4-5, a mixture of AFGP4 (18 kDa) and AFGP5 (11 kDa), as well as fish AFGP8 (n = 4), about 2.7 kDa, from *Trematomus borchgrevinki*[9] were used as AFP controls. Additionally, two other controls, denatured DAFP1 and GalNAc (the disaccharide moiety of AFGPs), were used in this study. All AFPs samples were applied at milli- and micro-molar concentrations.

Effects of AFGPs and other controls on D-mannitol crystallization

In the absence of any additives, the first appearance of precipitates from D-mannitol supersaturated solution occurred on day 14 (Table S1). The D-mannitol crystals grown from its supersaturated solution appeared as elongated rods along the *c* axis (Figures 2A and 2B), which is a characteristic shape of β-form D-mannitol. The addition of either control (GalNAc or denatured DAFP1) did not affect the crystallization of D-mannitol: we observed the same induction time, appearance, and weights of the finally achieved D-mannitol crystals from these samples in the presence of the controls. The addition of AFGPs affected D-mannitol crystallization from its supersaturated solution to varying degrees. The presence of 1.0×10^{-2} molar AFGP4-5 or AFGP8 delayed the first appearance of D-mannitol precipitates by 49 or 27 days, leading to less amounts of the final crystals at the stop time (Table S1). The crystal habits remained the same, although they appeared as relatively smaller elongated rods. The inhibitory effect of AFGP4-5 on D-mannitol crystallization was more significant than that of AFGP8, in that higher concentrations of AFGP4-5 had a

Author Manuscript Author Manuscript Author Manuscript Author Manuscript

more pronounced effect in delaying the induction time of D-mannitol crystallization. Such concentration effects were not obvious for AFGP8. For effective inhibition of crystallization, interactions between the additive and the compound of interest are generally required.[3] The results of AFGP8 are more similar to those of the negative controls, indicating that AFGP8 has low affinity to D-mannitol. These results also suggest that the crystallization of D-mannitol can only be affected by AFGPs to a very limited extent, and which may be through weak suppression of the crystal growth of D-mannitol.

The final crystals were all checked using single crystal X-ray diffraction and confirmed to be β-form D-mannitol. Specifically, the crystallographic data (Table S2) of D-mannitol crystals achieved in the presence of denatured DAFP1 were analyzed and deposited in the Cambridge Crystallographic Data Center (CCDC number: 2015391). These results are in good accordance with those published previously[20] and were used for the structural analysis herein (Table S2 and the supplemental experimental procedures).

To characterize subtle differences in the hydrogen bonding (HB) arrangements of the final D-mannitol solids, we utilized ^{13}C cross-polarization magic angle spinning (CP-MAS) NMR spectroscopy (Figure 2C) and attenuated total reflectance Fourier-transform infrared (ATR-FTIR; Figure S1 and the supplemental experimental procedures) spectroscopy. The spectra of the D-mannitol solids achieved in the presence of the AFGPs and the controls were identical to those of the D-mannitol solids obtained in the absence of additives, which are in good agreement with published data for β-form D-mannitol,[21] indicating that all crystallites are pure β-form D-mannitol. Thus, it is possible that AFGPs may to some extent suppress the continued crystal growth of D-mannitol, but there is no apparent adsorption of AFGPs on the crystal surfaces of D-mannitol.

Complete inhibition of D-mannitol nucleation by micromolar DAFP1

In contrast to all the controls including AFGPs, DAFP1 showed a dramatic inhibition of nucleation of D-mannitol from its highly supersaturated aqueous solution (Figure 2D). Notably, potential effects of DAFP1 on the supersaturation degree of D-mannitol have been ruled out by the control experiments (Table S1) and then confirmed by the seeding experiments (Figure S2 and the supplemental experimental procedures). Moreover, Figure S2 shows that DAFP1 can effectively reduce the growth speed of the D-mannitol crystals with an inhibitory effect that is much more significant than that of AFGPs. This suggests that when seed crystals are present, DAFP1 can also reduce the rate of crystal growth, slowing down crystallization of D-mannitol. Indeed, no crystallization of D-mannitol in the presence of DAFP1 has been observed after more than 3 years' storage despite the lower, micro-molar (2.8×10^{-6} M) concentration. Furthermore, the structural integrity of D-mannitol was assessed by NMR spectroscopy. ^{1}H and ^{13}C NMR spectra (Figures S3 and S4 and the supplemental experimental procedures) confirm the integrity of the 3-year-old D-mannitol structure, which rules out the possibility that the lack of crystallization was due to the loss of the structural integrity of D-mannitol in the solution. Thus, this dramatic suppression of nucleation is unprecedented in terms of the level of the additive used and the duration.

Author Manuscript Author Manuscript Author Manuscript Author Manuscript

D-mannitol solutions can be highly supersaturated by cooling,[15,22] and the metastable zone width (MSZW) of D-mannitol is narrow across a wide temperature range[14] suggesting that the 1 M D-mannitol at 4°C exceeds the critical supersaturation of D-mannitol for nucleation. Indeed, we observed D-mannitol crystallization in 2 weeks in the absence of additives (Figure 2). How can micromolar DAFP1 suppress the nucleation of highly supersaturated 1 M D-mannitol solutions for over 3 years? Inhibition by adsorption,[1,23] the generally accepted mechanism for crystallization inhibition, cannot explain this phenomenon because there are no crystal growth for D-mannitol in the presence of DAFP1. Further, at 1 M concentration, our D-mannitol solutions at 4°C are far above the critical saturation point, which rules out the possibility that the observed inhibition arises from enhanced solubility due to the addition of DAFP1 at a micromolar level. Thus, we postulated that DAFP1 must somehow reduce dramatically the concentration of the key conformation required for forming the nucleus and a major conformer with a dimer network on the fastest growth faces of the D-mannitol crystal is the key crystal forming rotamer (CFR).

Stable D-mannitol conformers and their interactions with DAFP-1 *in silico*

In order to discover the atomistic mechanism underlying the nucleation inhibition of D-mannitol by DAFP1, we carried out a series of molecular dynamics (MD) simulations. The chiral D-mannitol molecule has 5 C – C backbone bonds, leading to $3^5 = 243$ possible stable conformations of the O-C-C-O torsional angles (Table S3), where the torsional angles are near trans (t = 180°), positive gauche (p = −60°) or negative gauche (n = −60°). Free energy analysis reveals that the T-T-P-T-T rotamer (BR) is the most favorable in the bulk solution at 277K, comprising 33.7% of the population. In contrast, the crystal forming rotamer (CFR) is N-T-P-T-N with just a 0.45% population. There is typically a large barrier for torsional rotation in the bulk solution, which precludes rapid conformational switching (Figure S5). Indeed, accelerated MD simulations[24,25] show barriers for internal β and δ torsional rotations of ~80 kJ/mol (Figure S6).

Classic nucleation theory[26] posits that spontaneous crystal growth from solution will occur once a critical nucleus size forms by stochastic collisions of the (specific rotamer) molecules necessary for crystallization. The critical nucleus size is the point of vanishing chemical potential; i.e., $\mu = (\partial G_{ex}/\partial N)_{T,P} = 0$. We verified that the nucleation kinetics of D-mannitol in the bulk solution is indeed classic[27] by considering clusters with up to 70 molecules. While simulations capable of capturing the kinetics of nucleation on realistic timescales remains a grand challenge,[28] we advance an approach here whereby we apply harmonic restraints to the center of mass of each molecule, in motifs seeded from the experimental crystal structure and calculate the excess Gibbs energy from equilibrium MD simulations combined with analysis using the two-phase thermodynamics method.[29] Our simulations finds a critical nucleus size of N = 64 molecules (Figure 3). Indeed, unrestrained MD simulations showed that clusters with less than 64 molecules were unstable on the nano-second timescale of our MD simulations, while simulations with clusters of more than 64 molecules were stable (Figure S7 and the supplemental experimental procedures). We calculated a Gibbs binding energy of $\Delta G_{bind} = -120 \pm 5$ kJ/mol at 277K for binding the key crystal forming rotamer to the (110) fast-growing crystal face, and we calculated a solid/liquid interfacial surface

Author Manuscript Author Manuscript Author Manuscript Author Manuscript

tension $\gamma = 34 \pm 4$ mJ/m^2. The calculated surface tension is within range of the experiment measurements[30]: 38 – 40 mJ/m^2 at room temperature (Table S4).

Previous studies of freezing point depression by AFPs suggested that the IBS of AFPs interacts directly with the growing ice face to block growth[23,31] or by a longer range effect whereby the vibrational dynamics of local water molecules are modified.[5] However with micromolar concentrations of DAFP1, these mechanisms cannot explain the inhibition of 1M D-mannitol nucleation observed here. Thus to discover the mechanism, we first predicted[32] the low-energy binding sites on DAFP1 for the CFR. We found two distinct binding sites with $\Delta E_{bind} = \sim -75$ kJ/mol (Table S5), each stabilized by at least 2 strong hydrogen bonds (HBs) to THR residues (Figure S8). The best binding pose was stabilized through HBs with the highly conserved T51, T53, T63, T65, and T77 residues on the well-defined IBS of DAFP1. Notably, the binding of other rotamers, specifically the BR, to DAFP1 is significantly less favorable than the CFR, due primarily to less favorable HBs.

The catch switch and release mechanism for complete D-mannitol nucleation inhibition by DAFP1

Extensive MD simulations, with the CFR D-mannitol confined to the IBS of DAFP1 in explicit solvent, revealed strong binding to the IBS (Figure 4A). Here, the D-mannitol molecule walks randomly along the IBS backbone during MD due to thermal fluctuations, after an initial 5 ns delay during which the bound D-mannitol adjusts to the solvent environment. Notably, the *Cis* configurations for some of the D-mannitol O-C-C-O torsional angles are stabilized (see the spikes at 0° for all 5 dihedrals in Figure S9 and the supplemental experimental procedures), due to enhanced H-bonding to DAFP1 (Figure 4B), dramatically reducing barriers for torsional transitions (Figure S10 and the supplemental experimental procedures). In fact, we find that D-mannitol on the DAFP1 surface switches conformations at a rate of 10 THz (Figure 4B). Although *Cis* configurations lead to high internal energy for the isolated D-mannitol, they increase HBs with adjacent hydrophilic groups on the DAFP1 IBS. Thus, the nanoscale architecture of the IBS of DAFP1, with ladder-like placement of THR and SER groups, facilitates new HBs to the key CFR, causing the rapid conformational switching that depresses the population of the D-mannitol CFR. Notably, we find that the structure of the IBS is generally well preserved, even while binding the D-mannitol (Figure S11 and the supplemental experimental procedures), consistent with X-ray crystallography studies that show that all the side chains of the THR residues have identical conformations. The net result is rapid switching to new conformations, with two distinct, otherwise high-energy, conformations particularly favored on the DAFP1 surface: #193: N-N-N-P-N (1.2%) and #185: N-P-T-N-P (1.0%) (Figure 4C). This nanoscale architecture, that facilitates the rapid conformer switching, is destroyed in the denatured DAFP1 and is not present in either AFGP4-5 or AFGP8, which explains why the AFGPs did not have the same nucleation inhibitory ability.

We further quantified the binding thermodynamics of the various rotamers to DAFP1 by means of accelerated MD simulations, which showed a Gibbs energy of binding $\Delta G_{bind} = -20.5$ kJ/mol for the CFR. In contrast, the binding free energy of two of the most likely conformers on the DAFP1 surface, #185 and #193, have unfavorable binding energies of

Author Manuscript Author Manuscript Author Manuscript Author Manuscript

ΔG_{bind} = +14.5 and +22.0 kJ/mol, respectively, and relatively modest desorption barriers: $\Delta G^{\#}$ = +3.0 and +3.5 kJ/mol respectively (Figure S12 and the supplemental experimental procedures). Unrestrained MD simulations support our free energy analysis: we find 3 desorption events over 100 ns of MD simulation, all of which were initiated by either rotamer #193 or #185. Overall, the computational results are summarized as the catch switch and release (CSaR) mechanism (Figure 5): DAFP1 preferentially binds the CFR molecule in the bulk solution, randomizes the torsions, and populates unfavorable configurations that desorb stochastically from the surface. Due to the large torsional rotational barriers in the bulk, these unfavorable configurations have relatively long lifetimes. The net result is that the total population of CFR molecules in the bulk is reduced by over three orders of magnitude, from 0.45% to ~2.0×10^{-4}% (Table S6 and the supplemental experimental procedures). Thus, the CSaR mechanism explains that micromolar DAFP1 is sufficient to inhibit D-mannitol nucleation. Assuming a linear relationship between the concentration and nucleation rate,[26] we predict that this reduction in the CFR population would extend the timescale for forming the critical nucleus from 14 days to nearly ~75 years.

In summary, we demonstrated experimentally that the stability of a highly supersaturated D-mannitol solution can be extended very dramatically by a hyperactive insect AFP, DAFP1, at a micromolar level. Extensive computer simulations suggest a new molecular mechanism that elucidates the origin for this unprecedented effect. These results advance a previously unreported and underappreciated role of AFPs in stabilizing highly supersaturated osmolyte solutions, suggesting new applications for these natural polymers. For example, isoforms of DAFP in the hemolymph of *D. canadensis,*[33] which are expected to have similar nanoscale architecture as that of DAFP1, may be other potential effective nucleation inhibitors for D-mannitol or analogs. It should also be noted that DAFP1 is used as an external additive here and may need to be removed from the D-mannitol solution through ultrafiltration until the safety of its inclusion is fully evaluated. By revealing the inventiveness of nature, these findings also suggest new design principles in controlling the crystal nucleation processes (especially those of small organic compounds), where conformers play a key role.

EXPERIMENTAL PROCEDURES

Resource availability

Lead contact—Further information and requests for resources should be directed to and will be fulfilled by the lead contact, Xin Wen (xwen3@calstatela.edu).

Materials availability—This study did not generate new unique materials.

Data and code availability—The data that support the findings of this study will be made available over the web. In-house programs that implement the two-phase thermodynamics method are available from the corresponding authors upon request. Modification to the LAMMPS simulation engine used in this study will be submitted to the original developers for inclusion in the official release.

Author Manuscript Author Manuscript Author Manuscript Author Manuscript

Materials

Chemicals were purchased from Sigma-Aldrich (St. Louis, MO) at ACS grade or better, except β-D-galactopyranosyl-(1- >3)-2-acetamido-2-deoxy-α-D-galactopyranose (GalNAc, analytical grade) was ordered from Santa Cruz Biotechnology (Santa Cruz, CA) and were used without additional purifications. In particular, solvents and chemicals for the HPLC experiments were purchased at HPLC grade from Sigma-Aldrich (St. Louis, MO). Aqueous solutions were prepared using Milli-Q water produced from a Synergy water system (Millipore) with a minimum resistivity of 18 MΩ•cm. Unless otherwise indicated, all of the samples including the proteins and peptide samples were filtered through 0.1 mm filters before use. Sample vials (8 mL, National Scientific) were purchased for crystallization. All glassware and stir bars used for crystallization were extensively washed. Briefly, they were first cleaned in a KOH/2-propanol bath. After rinsed with distilled water, they were soaked in 1 M HCl for 24 h. After rinsed with distilled water, they were finally cleaned using RBS 35 (Thermo Fisher), a surface-active detergent. After rinsed with distilled water and then with deionized water thoroughly, the washed glassware and stir bars were air-dried at room temperature before use.

Antifreeze proteins preparation

DAFP1, an AFP from *Dendroides canadensis,* was expressed and purified as described previously.[12] Briefly, the protein was expressed as a fusion protein in *Escherichia coli.* The cells were harvested by centrifugation at 4°C. After the cells were disrupted, the crude protein was purified using immobilized metal ion affinity chromatography (IMAC) (Ni-NTA agarose, QIAGEN). The tags of the AFP were cleaved off enzymatically and the tag-free protein was further purified by using IMAC and ion exchange chromatography. The purified DAFP1 was characterized by the matrix-assisted laser desorption ionization time-of-flight (MALDI-TOF) mass spectrometry, circular dichroism spectrometry, and differential scanning calorimetry as described previously,[34] and the identity of DAFP1 was confirmed. The purity of DAFP1 was assessed by high-performance liquid chromatography (HPLC) with a purity higher than 95%. The concentration of stock DAFP1 solution or stock denatured DAFP1 was determined using a Cary 100 Bio UV-Vis spectroscopy (Varian) and the extinction coefficient of $5.47 \times 10^3\ M^{-1}cm^{-1}$ at 280 nm was used.[34] The denatured DAFP1 with completely reducing its disulfide bonds was prepared following a known methods.[10] Briefly, 1.0 mM purified DAFP1 was incubated in 0.10 M sodium citrate, pH 3.00, and 15.0 mM tris(2-carboxyethyl)phosphine hydrochloride (TCEP) for 30 min at 60 °C. The denatured DAFP1 was purified using ÄKTA Purifier 10 (GE Healthcare) with a Sephacryl S-100 gel filtration column (GE Healthcare). Antifreeze glycoproteins, AFGP4–5 and AFGP8 from the Antarctic notothenioid *Trematomus borchgrevinki,*[9] were gifts from Professor Yin Yeh (UC Davis). The AFGPs were received as lyophilized powders and were used without further purification. All the weight measurements for AFGPs were carried out with an Ohaus Voyager Pro analytical and precision balance (Parsippany, NJ).

Crystal growth procedure

Slow evaporation of a D-mannitol aqueous solution can yield β-form D-mannitol crystals, but it produces large amounts of microcrystals.[20] In order to yield pure β-form D-mannitol

Author Manuscript Author Manuscript Author Manuscript Author Manuscript

crystals without microcrystals, we tested many crystallization conditions and found that lowering the growth temperature can eliminate the microcrystals and yield large pure β form D-mannitol crystals. The test was repeated seven times and the crystallization of D-mannitol alone was reproducible with respect to the sizes, shapes, and final weights of the final crystals. The developed crystallization conditions were then used in the following experiments for D-mannitol alone and in the presence of AFPs and controls, respectively.

Briefly, on day 1,20 μL of either water or 2-acetamido-2-deoxy-3-O-(β-D-galactopyranosyl)-D-galactose, denatured DAFP1, DAFP1, AFGP4-5, and AFGP8 solutions at specific concentrations, respectively, were added into each sample vial containing 2.00 mL of supersaturated D-mannitol aqueous solution. The final D-mannitol concentration was 1.00 M in each vial. The final molar ratios of the controls (i.e., GalNAc, denatured DAFP1) to D-mannitol were 1.0×10^{-2} in the vials. The final molar ratios of AFPs to D-mannitol in the vials were either 1.0×10^{-2} or 2.8×10^{-6} for DAFP1; and either 1.0×10^{-2} or 2.8×10^{-5} for AFGP4-5 or for AFGP8. The vials were gently swirled after the additions. The sample vials were then tightly closed using caps and stored at 4 °C. Three observations were recorded for each vial every day since day 1 until no apparent growth of crystals was observed. The intervals between two consecutive observations were about 8 h, but not less than 6 h. All the experiments were repeated seven times. Sample results were listed in Table S1.

The crystallization in the vials except those in the presence of DAFP1 were stopped after 200 days at 4°C by separating the mother liquor from the formed crystals. The vials were then warmed up to room temperature and photos of the vials were taken. The crystals were dried at room temperature for optical microscopy and other characterizations. Microscopic observations were performed with a Nikon SMZ-1000 polarizing microscope equipped with a DS-Fi2 color camera after the crystallization were completed. The weights of the achieved crystals were analyzed for five experiments in comparison to the total amounts of D-mannitol added into the vials, and the average values were listed in Table S1.

NMR spectroscopy

Solid-state ^{13}C cross-polarized magic angle spinning (^{13}C CP/MAS) NMR spectra were recorded at 298 K at 75.47 MHz (^{13}C) on a Bruker spectrometer using a 4 mm broadband MAS probe with proton broadband decoupler. Approximately 120 mg of solids were gently ground using mortar and pestle and packed in a 4 mm wide ZrO_2 rotor with a Kel-F cap. Spinning frequency of 10 kHz, CP contact time of 1.5 ms, and a 60 s delay were utilized.

Equilibrium MD simulations

Molecular dynamics (MD) simulations were performed using LAMMPS.[35] The D-mannitol molecule was described with the CHARMM carbohydrates forcefield,[36] with parameters obtained from the Ligand reader and modeler input generator[37] on the CHARMM-GUI web portal.[38] The water molecules were described using the TIP4P-ice water model.[39] The DAFP1 starting structure was obtained from our previous work[34] and described here in fully atomistic detail using the CHARMM36m[40] plus CMAP[41] forcefields.

Author Manuscript Author Manuscript Author Manuscript Author Manuscript

In each simulation, we employed a 1.2 nm distance cutoff for the van der Waals interaction, where the energy and forces after 1.0 nm go smoothly to zero using a cubic spline switching function. The real space cutoff for the electrostatics was also 1.2 nm, and the long-range electrostatic interactions were obtained from the particle-particle particle-mesh method,[42] with a force tolerance of 10^{-6}.

In our equilibration MD procedure, we first performed an initial energy minimization at 0 K and then slowly heated from 0 K to 277K at constant volume over 0.5 ns using a Langevin thermostat, with a damping parameter of 100 ps. The system was then subjected to 5 cycles of quench-annealing dynamics, with a 500 kcal/mol/$Å^2$ spring applied to the protein/ligand complex to keep it from moving. After annealing, the restraints were removed and the system was equilibrated using the constant temperature (277 K), constant pressure (1 bar) (NPT) ensemble for 1 ns. Finally, we simulated the system in the NVT ensemble for at least 20 ns, saving snapshots of the system (atomic positions and coordinates) every 1ps.

Accelerated meta-dynamics simulations

We explored the rugged free energy landscape for three systems using well-tempered[43], multiple walker[44] metadynamics[24,45,46]: (1) the β, δ torsional rotation 2D PES of D-mannitol in the bulk solvent, (2) the 2D PES of D-mannitol confined to the DAFP1 surface, and (3) the binding thermodynamics various D-mannitol rotamers to the DAFP1 binding site 1. In all cases, we use 10 walkers, each initiated from various points along the equilibrium production MD trajectory. In cases 2 and 3, we further accelerated convergence by restraining the motions of the D-mannitol molecule using the funneling approach.[47] In case 3, we separately considered the various rotamers by constraining the D-mannitol internal structure using rigid body dynamics.[48]

In each simulation, MW-wt-MetaD biases were constructed as follows: Gaussian functions were deposited every 0.5 ps with an initial height of 277/T x 1.0 kcal/ mol. The bias factor [$g = (T + \Delta T) / T$] was set to 5. The widths were 0.01 and 0.1 for the torsion rotation barriers and the center of mass distance between the DAFP1 and D-mannitol, respectively. We monitored convergence by calculating the free energy profiles every 1 ns and found that ~30 ns was reasonable in most cases. All simulations were performed using LAMMPS and Plumed 2.5.[49-51]

Supplementary Material

Refer to Web version on PubMed Central for supplementary material.

ACKNOWLEDGMENTS

Experimental portions of this work were performed at California State University, Los Angeles. We would like to thank Prof. Yin Yeh at the University of California, Davis for AFGPs, Prof. John Duman at University of Notre Dame for cDNA of DAFP1, and Dr. Ignacio Martini and Dr. Robert Taylor at the University of California, Los Angeles, for molecular instruments supported by the National Institutes of Health – the National Center for Research Resources under S10-RR025631. X.W. acknowledges supports from the National Institutes of Health (NIH grant number SC3GM086249) and the National Science Foundation (NSF grant number 1840835). A.K. acknowledges supports from NIH MARC U*STAR (T34GM008228) and NSF LSAMP-BD (HRD-1700556) at Cal State LA. WAG acknowledges support from NSF (CBET-2005250). T.A.P. also acknowledges fruitful discussions and support from N.M., L.F.P., and V.A.P. and support from the JSOE startup fund at UCSD. This research

Author Manuscript Author Manuscript Author Manuscript Author Manuscript

was partially supported by NSF through the UC San Diego Materials Research Science and Engineering Center (UCSD MRSEC DMR-2011924). Computational support for this work was provided in part by the National Energy Research Scientific Computing Center (NERSC), a U.S. Department of Energy Office of Science User Facility operated under Contract No. DE-AC02-05CH11231. Theoretical portions of work were performed as a user project at the Molecular Foundry, Lawrence Berkeley National Laboratory supported by the Office of Science, Office of Basic Energy Sciences, of the U.S. Department of Energy under the same contract. This work also used the Extreme Science and Engineering Discovery Environment (XSEDE) from allocation DDP381 on the Comet and Expanse supercomputers at the San Diego Supercomputing center, which is supported by National Science Foundation grant number ACI-1548562.

REFERENCES

1. Weissbuch I, Addadi L, Lahav M, and Leiserowitz L (1991). Molecular recognition at crystal interfaces. Science 253, 637–645. [PubMed: 17772367]
2. Liou Y-C, Tocilj A, Davies PL, and Jia Z (2000). Mimicry of ice structure by surface hydroxyls and water of a β-helix antifreeze protein. Nature 406, 322–324. [PubMed: 10917536]
3. Myerson AS, Erdemir D, and Lee AY (2019). Handbook of Industrial Crystallization, Third Edition (Cambridge University Press).
4. Duman JG (2015). Animal ice-binding (antifreeze) proteins and glycolipids: an overview with emphasis on physiological function. J. Exp. Biol 218, 1846–1855. [PubMed: 26085662]
5. Meister K, Ebbinghaus S, Xu Y, Duman JG, DeVries A, Gruebele M, Leitner DM, and Havenith M (2013). Long-range protein-water dynamics in hyperactive insect antifreeze proteins. Proc. Natl. Acad. Sci. USA 110, 1617–1622. [PubMed: 23277543]
6. Wen X, Wang S, Duman JG, Arifin JF, Juwita V, Goddard WA 3rd, Rios A, Liu F, Kim S-K, Abrol R, et al. (2016). Antifreeze proteins govern the precipitation of trehalose in a freezing-avoiding insect at low temperature. Proc. Natl. Acad. Sci. USA 113, 6683–6688. [PubMed: 27226297]
7. Franks F (1985). Biophysics and Biochemistry at Low Temperatures (Cambridge University Press).
8. DeVries AL (1971). Glycoproteins as biological antifreeze agents in antarctic fishes. Science 172, 1152–1155. [PubMed: 5574522]
9. Feeney RE, and Yeh Y (1978). Antifreeze proteins from fish bloods. In Advances in Protein Chemistry, Anfinsen CB, Edsall JT, and Richards FM, eds. (Academic Press), pp. 191–282.
10. Wang S, Wen X, Nikolovski P, Juwita V, and Arifin JF (2012). Expanding the molecular recognition repertoire of antifreeze polypeptides: effects on nucleoside crystal growth. Chem. Commun. (Camb.) 48, 11555–11557. [PubMed: 23089878]
11. Wang S, Wen X, DeVries AL, Bagdagulyan Y, Morita A, Golen JA, Duman JG, and Rheingold AL (2014). Molecular recognition of methyl α-D-mannopyranoside by antifreeze (glyco)proteins. J. Am. Chem. Soc 136, 8973–8981. [PubMed: 24918258]
12. Amornwittawat N, Wang S, Banatlao J, Chung M, Velasco E, Duman JG, and Wen X (2009). Effects of polyhydroxy compounds on beetle antifreeze protein activity. Biochim. Biophys. Acta 1794, 341–346. [PubMed: 19038370]
13. Chippendale GM (1978). The functions of carbohydrates in insect life processes. In Biochemistry of Insects, Rockstein M, ed. (Academic Press), pp. 1–55.
14. Bensouissi A, Roge B, and Mathlouthi M (2010). Effect of conformation and water interactions of sucrose, maltitol, mannitol and xylitol on their metastablezone width and ease of nucleation. Food Chem. 122, 443–446.
15. Kavanagh O, Hogan F, Murphy C, Croker D, and Walker G (2020). Formulating a Stable Mannitol Infusion while Maintaining Hyperosmolarity. Pharmaceutics 12, 187.
16. Anderson SD, Daviskas E, Brannan JD, and Chan HK (2018). Repurposing excipients as active inhalation agents: The mannitol story. Adv. Drug Deliv. Rev 133, 45–56. [PubMed: 29626547]
17. Mannitol Intravenous (Mannitol Injection, USP). (2019). https://www.accessdata.fda.gov/drugsatfda_docs/label/2019/016269s055lbl.pdf.
18. Izutsu K, Yoshioka S, and Terao T (1993). Decreased protein-stabilizing effects of cryoprotectants due to crystallization. Pharm. Res 10, 1232–1237. [PubMed: 8415413]

Author Manuscript Author Manuscript Author Manuscript Author Manuscript

19. Kosan J, and Gieseler H (2020). Freeze Drying of Vaccines – Challenges and Concepts in Formulation and Process Development SP Scientific Webinar Tech Note. https://www.spscientific.com/WebinarDetail.aspx?id=4576.
20. Fronczek FR, Kamel HN, and Slattery M (2003). Three polymorphs (alpha, beta, and delta) of D-mannitol at 100 K. Acta Crystallogr. C 59, O567–O570. [PubMed: 14532673]
21. Grindley TB, McKinnon MS, and Wasylishen RE (1990). Towards understanding 13C-N.M.R. chemical shifts of carbohydrates in the solid state. The spectra of d-mannitol polymorphs and of dl-mannitol. Carbohydr. Res 197, 41–52.
22. Yi Y, Hatziavramidis D, Myerson AS,Waldo M, Beylin VG, and Mustakis J (2005). Development of a Small-Scale Automated Solubility Measurement Apparatus. Ind. Eng. Chem. Res 44, 5427–5433.
23. Raymond JA, and DeVries AL (1977). Adsorption inhibition as a mechanism of freezing resistance in polar fishes. Proc. Natl. Acad. Sci. USA 74, 2589–2593. [PubMed: 267952]
24. Ensing B, De Vivo M, Liu Z, Moore P, and Klein ML (2006). Metadynamics as a tool for exploring free energy landscapes of chemical reactions. Acc. Chem. Res 39, 73–81. [PubMed: 16489726]
25. Invernizzi M, and Parrinello M (2020). Rethinking Metadynamics: From Bias Potentials to Probability Distributions. J. Phys. Chem. Lett 11, 2731–2736. [PubMed: 32191470]
26. Kashchiev D (2006). Forms and applications of the nucleation theorem. J. Chem. Phys 125, 014502. [PubMed: 16863311]
27. Henzler K, Fetisov EO, Galib M, Baer MD, Legg BA, Borca C, Xto JM, Pin S, Fulton JL, Schenter GK, et al. (2018). Supersaturated calcium carbonate solutions are classical. Sci. Adv 4, eaao6283. [PubMed: 29387793]
28. Sosso GC, Chen J, Cox SJ, Fitzner M, Pedevilla P, Zen A, and Michaelides A (2016). Crystal nucleation in liquids: Open questions and future challenges in molecular dynamics simulations. Chem. Rev 116, 7078–7116. [PubMed: 27228560]
29. Lin ST, Blanco M, and Goddard WA (2003). The two-phase model for calculating thermodynamic properties of liquids from molecular dynamics: Validation for the phase diagram of Lennard-Jones fluids. J. Chem. Phys 119, 11792–11805.
30. Cares-Pacheco MG, Vaca-Medina G, Calvet R, Espitalier F, Letourneau JJ, Rouilly A, and Rodier E (2014). Physicochemical characterization of D-mannitol polymorphs: the challenging surface energy determination by inverse gas chromatography in the infinite dilution region. Int. J. Pharm 475, 69–81. [PubMed: 25151549]
31. Knight CA (2000). Structural biology. Adding to the antifreeze agenda. Nature 406, 249–251. [PubMed: 10917514]
32. Griffith AR (2017). DarwinDock and GAG-Dock: Methods and Applications for Small Molecule Docking. PhD thesis (California Institute of Technology).
33. Duman JG, Verleye D, and Li N (2002). Site-specific forms of antifreeze protein in the beetle Dendroides canadensis. J. Comp. Physiol. B 172, 547–552. [PubMed: 12192517]
34. Wang S, Amornwittawat N, Juwita V, Kao Y, Duman JG, Pascal TA, Goddard WA, and Wen X (2009). Arginine, a key residue for the enhancing ability of an antifreeze protein of the beetle Dendroides canadensis. Biochemistry 48, 9696–9703. [PubMed: 19746966]
35. Plimpton S (1995). Fast parallel algorithms for short-range molecular-dynamics. J. Comp. Physiol 117, 1–19.
36. Guvench O, Mallajosyula SS, Raman EP, Hatcher E, Vanommeslaeghe K, Foster TJ, Jamison FW 2nd, and Mackerell AD Jr. (2011). CHARMM additive all-atom force field for carbohydrate derivatives and its utility in polysaccharide and carbohydrate-protein modeling. J. Chem. Theory Comput 7, 3162–3180. [PubMed: 22125473]
37. Kim S, Lee J, Jo S, Brooks CL III, Lee HS, and Im W (2017). CHARMM-GUI ligand reader and modeler for CHARMM force field generation of small molecules (Wiley Online Library).
38. Jo S, Kim T, Iyer VG, and Im W (2008). CHARMM-GUI: a web-based graphical user interface for CHARMM. J. Comput. Chem 29, 1859–1865. [PubMed: 18351591]
39. Abascal JLF, Sanz E, García Fernández R, and Vega C (2005). A potential model for the study of ices and amorphous water: TIP4P/Ice. J. Chem. Phys 122, 234511. [PubMed: 16008466]

Author Manuscript Author Manuscript Author Manuscript Author Manuscript

40. Huang J, Rauscher S, Nawrocki G, Ran T, Feig M, de Groot BL, Grubmüller H, and MacKerell AD Jr. (2017). CHARMM36m: an improved force field for folded and intrinsically disordered proteins. Nat. Methods 14, 71–73. [PubMed: 27819658]
41. Mackerell AD Jr., Feig M, and Brooks CL 3rd (2004). Extending the treatment of backbone energetics in protein force fields: limitations of gas-phase quantum mechanics in reproducing protein conformational distributions in molecular dynamics simulations. J. Comput. Chem 25, 1400–1415. [PubMed: 15185334]
42. Hockney RW, and Eastwood JW (1988). Computer Simulation Using Particles, First Edition (Taylor & Francis Group).
43. Barducci A, Bussi G, and Parrinello M (2008). Well-tempered metadynamics: a smoothly converging and tunable free-energy method. Phys. Rev. Lett 100, 020603. [PubMed: 18232845]
44. Raiteri P, Laio A, Gervasio FL, Micheletti C., and Parrinello M (2006). Efficient reconstruction of complex free energy landscapes by multiple walkers metadynamics. J. Phys. Chem. B 110, 3533–3539. [PubMed: 16494409]
45. Laio A, and Parrinello M (2002). Escaping free-energy minima. Proc. Natl. Acad. Sci. USA 99, 12562–12566. [PubMed: 12271136]
46. Barducci A, Bonomi M, and Parrinello M (2011). Metadynamics. WIREs Computational Molecular Science 1, 826–843.
47. Limongelli V, Bonomi M, and Parrinello M (2013). Funnel metadynamics as accurate binding free-energy method. Proc. Natl. Acad. Sci. USA 110, 6358–6363. [PubMed: 23553839]
48. Kamberaj H, Low RJ, and Neal MP (2005). Time reversible and symplectic integrators for molecular dynamics simulations of rigid molecules. J. Chem. Phys 122, 224114. [PubMed: 15974658]
49. Bonomi M, Bussi G, Camilloni C, Tribello GA, Banáš P, Barducci A, Bernetti M, Bolhuis PG, Bottaro S, and Branduardi D; PLUMED consortium (2019). Promoting transparency and reproducibility in enhanced molecular simulations. Nat. Methods 16, 670–673. [PubMed: 31363226]
50. Tribello GA, Bonomi M, Branduardi D, Camilloni C, and Bussi G (2014). PLUMED 2: New feathers for an old bird. Comput. Phys. Commun 185, 604–613.
51. Bonomi M, Branduardi D, Bussi G, Camilloni C, Provasi D, Raiteri P, Donadio D., Marinelli F, Pietrucci F, and Broglia RA (2009). PLUMED: A portable plugin for free-energy calculations with molecular dynamics. Comput. Phys. Commun 180, 1961–1972.

Author Manuscript Author Manuscript Author Manuscript Author Manuscript

Highlights

- Spontaneous crystallization of a polyol is halted by a natural biopolymer
- The insect antifreeze protein (DAFP1) completely inhibits D-mannitol nucleation
- DAFP1 recognizes and reduces D-mannitol crystal forming rotamer (CFR) in solution
- The reduction in the CFR population in solution extends the nucleation time

Author Manuscript Author Manuscript Author Manuscript Author Manuscript

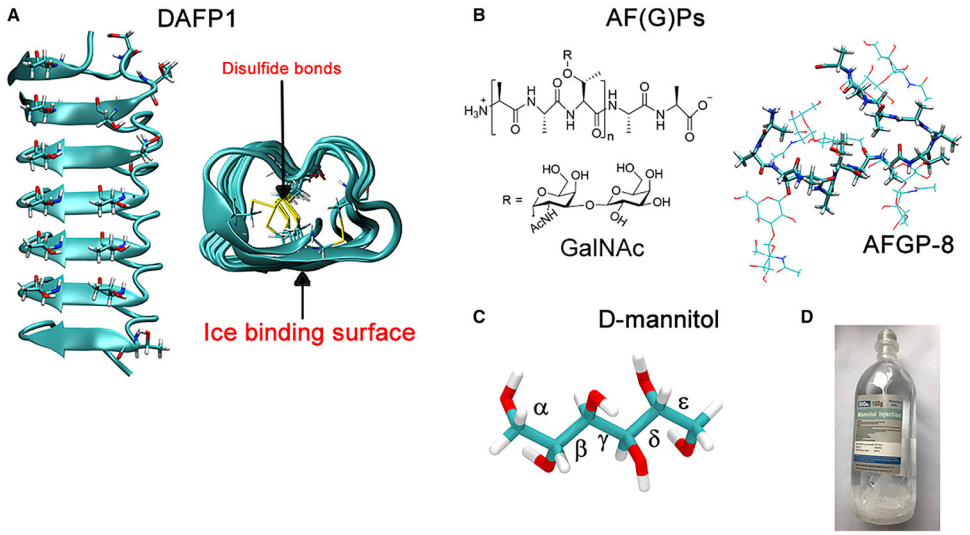

Figure 1. AF(G)P molecular structures

(A) Molecular model of DAFP1, where threonine and serine residues on the ice-binding sites (IBS) are shown as licorice. The intra-molecular di-sulfide bonds (cleaved in the denatured structure) are shown in the right inset, where the IBS is also indicated.

(B) Structure of AFGPs, where n = 4–55 and R = GalNAc. An atomistic representation in the right inset, where the amino-acid backbone is in licorice, and the GalNAc is shown in ball and stick.

(C) Molecular structures of D-mannitol, a stick-ellipsoid representation, showing each of the five O-C-C-O torsions (labeled α, β, γ, δ, and ε, respectively).

(D) Commercially available D-mannitol 20% injection solution with substantial D-mannitol crystals at the bottom of the bottle (the picture was shown on the company website).

Author Manuscript Author Manuscript Author Manuscript Author Manuscript

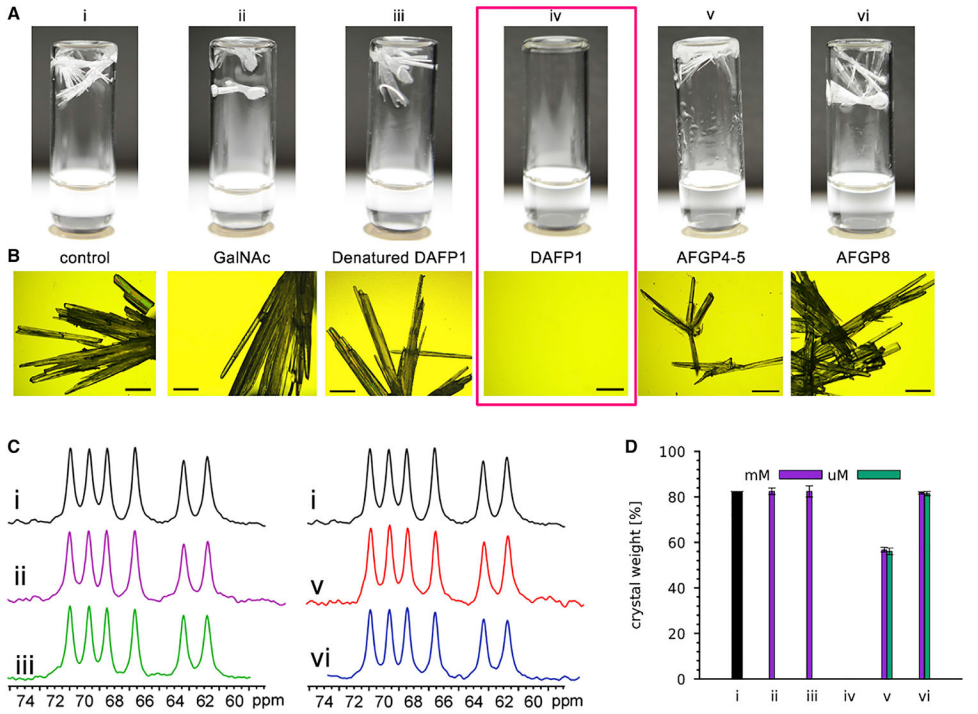

Figure 2. Experimental data for D-Mannitol crystal inhibition by various additives

(A) D-Mannitol crystals grown in the absence and presence of additives in vials (shown upside-down), pictured after at least 200 days. Note no crystals form in iv with 1 micromole of DAFP1.

(B) Representative optical micrographs of the obtained crystals. The scale bar represents the length of 2 mm. The ordering is the same as in (A). Note again no crystals form in iv with 1 micromole of DAFP1.

(C) The CP-MAS ^{13}C NMR spectra of finally achieved D-mannitol solids, using the same ordering as in (A). Since the DAFP1 sample has no solids, NMR spectrum of "i," D-mannitol alone, is re-used here for comparison.

(D) Comparison of D-mannitol crystal growth in the absence and presence of additives at milli- (purple) and micro-molar (green) concentrations. Micromolar concentrations of GalNAc and the denatured DAFP1 led to crystals similar to the millimolar concentrations and are omitted. Error bars are for standard deviations.

Author Manuscript Author Manuscript Author Manuscript Author Manuscript

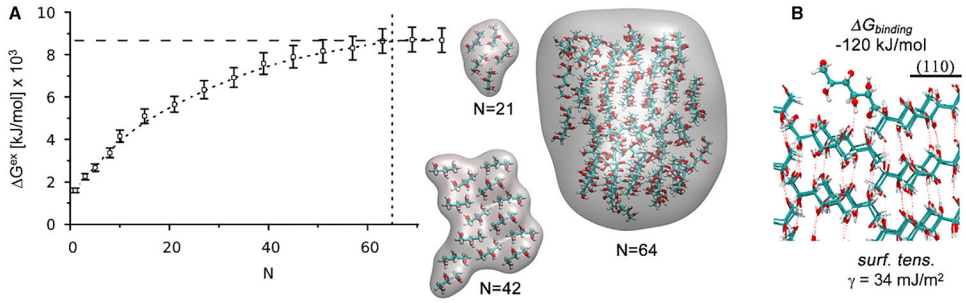

Figure 3. Thermodynamics of D-mannitol nucleation

(A) Excess Gibbs energy ΔG^{ex} of D-mannitol crystallites as a function of crystal size from restrained, equilibrium MD simulations analyzed with the 2PT Method. The results from our simulations (circles) are fitted to a natural log function (dashed line) to guide the eyes. The vertical dashed line at n = 64 is the predicted minimum crystallite size for spontaneous nucleation. Crystallites of up to 75 molecules were considered and found to have similar excess Gibbs energy to the 64 molecule case. The vertical dashed line is the Gibbs energy of a 2D periodic slab with the same number of D-mannitol molecules. Errors bars indicate the uncertainty in our calculated free energies (1 standard deviation) Insets: representative structures of various sized clusters.

(B) Representative atomistic structure of a D-mannitol molecule at the (110) fast growing crystal face. The water molecules are not shown for clarity.

Author Manuscript Author Manuscript Author Manuscript Author Manuscript

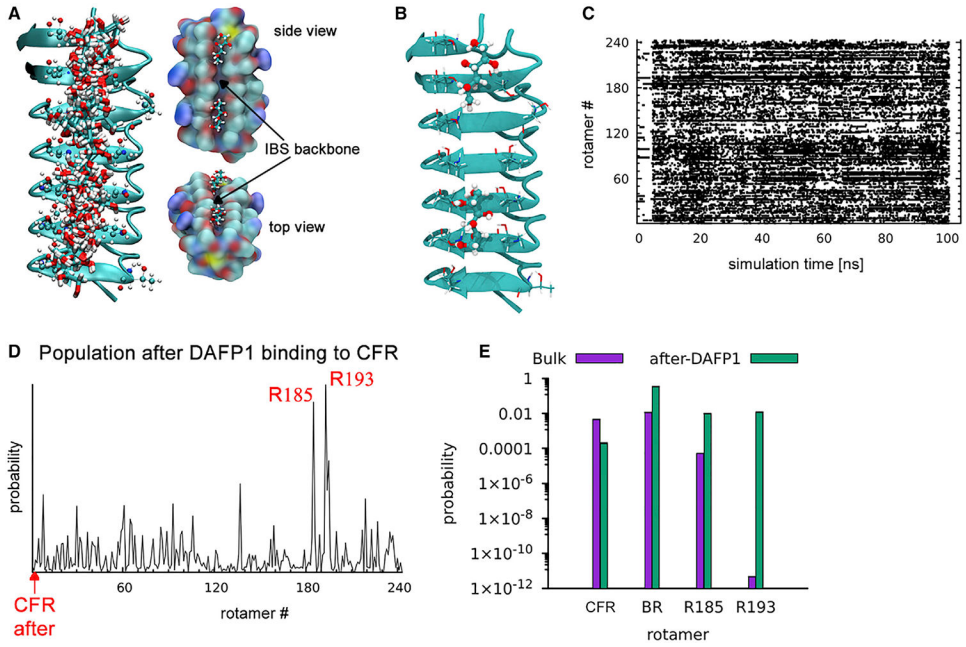

Figure 4. Mechanism of D-mannitol inhibition by DAFP1

(A) Molecular structure of D-mannitol in the IBS of DAFP1. Snapshots along our 100 ns MD simulations are superimposed, to demonstrate the mobility of D-mannitol along the backbone. Right insets: structure of two low energy binding sites. DAFP1 is represented by a surface electrostatic potential map.

(B) Molecular structure of D-mannitol bound to both sites on DAFP1, stabilized by hydrogen bonds.

(C) Rotamer map of a CFR molecule confined to the DAFP1 IBS.

(D) Rotamer population analysis of (C), showing that the DAFP1 significantly reduces the CFR (rotamer #1) population. The most probable rotamer (#185 and #193) are also indicated.

(E) Comparison of the predicated D-mannitol population at 277K in the bulk solution (purple bars) and after application of 1mM DAFP1 (green bars). Data for the crystal forming rotamer (CFR), best bulk rotamer (BR), and rotamers #185 and #193 are presented along with the calculated error bars (representing 1 standard deviation). Note the log scale on the y axis for the populations, where the CFR population is reduced by a factor of 2,500 in the presence of DAFP1 however the BR population is relatively unaffected.

Author Manuscript Author Manuscript Author Manuscript Author Manuscript

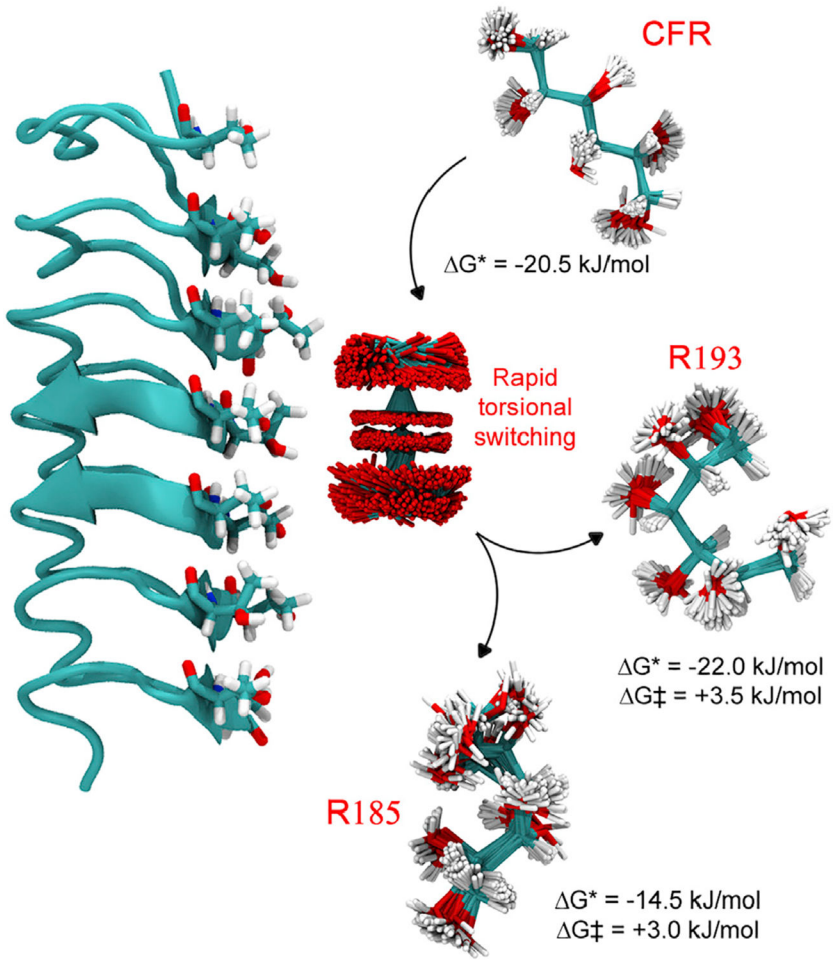

Figure 5. Molecular mechanism of D-mannitol crystallization by DAFP1

Schematic of catch switch and release (CSaR) mechanism. The molecular structures are shown. In the case of D-mannitol (ball and stick representation), the fluctuations in the structure are presented. The binding Gibbs energy (ΔG*) and activation barrier ($\Delta G^{\#}$) are reported.